
Scene-Adaptive Motion Planning with Explicit Mixture of Experts and Interaction-Oriented Optimization

Hongbiao Zhu[†]

Liulong Ma^{†,*}

Xian Wu

Xin Deng

Xiaoyao Liang

[†]These authors contributed equally to this work
Automotive New Technology Research Institute
BYD Company Limited

*Corresponding author: ma.liulong@byd.com

Abstract

Despite over a decade of development, autonomous driving trajectory planning in complex urban environments continues to encounter significant challenges. These challenges include the difficulty in accommodating the multi-modal nature of trajectories, the limitations of single expert in managing diverse scenarios, and insufficient consideration of environmental interactions. To address these issues, this paper introduces the EMoE-Planner, which incorporates three innovative approaches. Firstly, the Explicit MoE (Mixture of Experts) dynamically selects specialized experts based on scenario-specific information through a shared scene router. Secondly, the planner utilizes scene-specific queries to provide multi-modal priors, directing the model’s focus towards relevant target areas. Lastly, it enhances the prediction model and loss calculation by considering the interactions between the ego vehicle and other agents, thereby significantly boosting planning performance. Comparative experiments were conducted using the NuPlan dataset against the state-of-the-art methods. The simulation results demonstrate that our model consistently outperforms SOTA models across nearly all test scenarios.

1 Introduction

Autonomous driving trajectory planning has evolved over decades, with rule-based methods[12, 10, 51] providing fundamental safety assurances via predefined logic and heuristics. However, in complex urban settings, three significant limitations become apparent: (1) The manual construction of rules struggles to accommodate dynamic interactions and abrupt changes in road topology, resulting in unaddressed long-tail scenarios; (2) Rigid trajectory generation fails to mimic the adaptive behaviors of human drivers, such as dynamically adjusting following distances; (3) An exponential increase in maintenance costs arises from the “combinatorial explosion” of accumulating rules.

Conversely, data-driven approaches, including imitation learning[6, 7, 47, 11, 23], address edge cases like extreme weather and complex traffic, capturing human-like driving behaviors from expert data. Reinforcement learning [22, 19, 24] enables dynamic optimization through advanced reward mechanisms. These systems offer lower costs and faster iterations compared to rule-based alternatives.

Despite their benefits, two primary challenges persist in complex urban environments: 1) Urban driving demands highly multi-modal planning to address dynamic constraints and interactive intentions. Existing methods [20, 40, 6] generate multiple candidate trajectories but require post-processing modules to select the best modality. The complexity of scenarios like roundabouts and intersections further complicates this issue, with single-expert networks struggling to perform consistently across varied situations. 2) Traditional imitation learning employs static loss functions that neglect agent-ego interactions, leading to higher collision rates in dense traffic compared to rule-based methods.

To address these challenges, this paper presents an explicit MoE model that incorporates ego-agent interactions, scene-specific queries for multi-modal planning in urban scenarios. The contributions of this paper include the following three points.

- Propose an explicit Mixture of Experts (EMoE) architecture that employs a shared scene router for explicit scenario classification and selects corresponding experts based on the classification results. This approach simplifies the responsibilities and learning complexity of each expert, thereby reducing training difficulty and enhancing model performance.
- Propose a novel scene-specific query to enable the model to focus on area that the goal point is located. The query simultaneously provides prior information to the model at both the decision level and the modality level, allowing the model to achieve better training efficiency and performance with only a small number of queries.
- Introduce an Interaction-Oriented Loss that explicitly accounts for the interaction between the ego vehicle and surrounding agent within the loss function. Furthermore, the prediction of surrounding agents trajectories considers their interaction with the ego vehicle, which not only improves the prediction accuracy but also indirectly optimizes the scene encoding.

2 Related Work

Multi-modal modeling Multi-modality is a significant and persistent challenge for autonomous driving trajectory planning. Early approaches [49, 31, 9] overlooked the inherent multi-modal nature of driving scenarios, particularly anchor-free methods that relied solely on environmental and map information to predict future trajectories. Even recent end-to-end models like UniAD[20], specifically its motion former component, leverage map and object information to generate trajectories via anchor-free motion queries. However, these approaches risk modal collapse due to their limited capacity to represent diverse potential behaviors. Current state-of-the-art models are increasingly adopting anchor-based strategies. PLUTO[6] and MPNP[8] employ a semi-anchor approach, leveraging reference lines as lateral anchors and anchor-free queries longitudinally to approximate multi-modality. While achieving impressive performance, these methods are heavily dependent on accurate road feature and topology information. Critically, existing perception models, including end-to-end architectures, struggle to directly output reliable reference line information, requiring the addition of rule-based layers for generation. This reliance on rule-based preprocessing hinders practical deployment and end-to-end learning. Alternatively, VAD2[5] and Hydra MDP[30] utilize pre-generated trajectory libraries as anchors to cover a wide range of possible trajectory modalities. These methods select the optimal trajectory by scoring candidates. Further refinements, such as applying Gaussian Mixture Models (GMMs) to trajectory generation [4, 18] or sampling trajectories from predicted heatmaps [17, 16], aim to improve the distribution rationality and selection probability of generated trajectories. Multi-modal Motion[34] also leverages generated trajectories as anchors but introduces a region-specific training paradigm, selecting different regional anchors based on ground truth. Diffusion models are gaining traction in trajectory generation [27, 32] due to their inherent multi-modal capabilities. However, their accuracy, efficiency, and stability require further enhancement. Approaches that leverage generated trajectories as anchors involve a large number of anchor points and impose excessive constraints on the diversity of the final trajectories.

Consequently, researchers have explored using trajectory endpoints or destination points as anchors [13, 52, 39, 48]. MTR[39] directly generates trajectory endpoints by clustering ground truth data, leveraging endpoints as intent points with learnable position embeddings serving as static intent queries. GoalFlow[48], builds upon these approaches by directly generating trajectory endpoints as anchors. While endpoint anchors enhance trajectory interpretability and preserve multi-modality, current methods use a single anchor set for all scenes. Dense anchor sets increase computation, while sparse anchor sets limit modality. This paper introduces a model with scene-specific endpoint anchors, balancing anchor density and modality representation across diverse driving environments.

Furthermore, the complexity of urban scenarios presents unique challenges, as differences between scenes persist despite some common planning rules. STR2[41] address this by replacing the GPT2 backbone in STR[42] with an MoE architecture, substituting the feedforward network in the Transformer[45] with an MoE layer. This adaptation leverages MoE’s classification capabilities, significantly boosting performance in closed-loop simulations. MoE[25, 29], widely used in large language models like deepseek-v2[33], Qwen1.5[2], Switch Transformer[14] and Skywork-MoE[46], is apt for planning tasks that require scenario-specific strategies. However, traditional MoE’s unsuper-

vised expert selection often leads to imbalanced loads and reduced interpretability. While techniques like auxiliary load balancing losses, as proposed in Switch Transformer[14] and DeepSeek-V2[33], can mitigate this issue, they also distort the overall loss landscape and potentially compromise model generalization. Therefore, this paper introduces an improved MoE architecture tailored for trajectory planning, which is not only highly interpretable but also provides valuable insights into data collection strategies based on the performance of individual experts.

Interactive game modeling Modeling multi-agent interactions remains a critical challenge in autonomous driving trajectory planning. The mutual influence between the planned trajectory and predicted trajectories presents fundamental complexity. Prediction-first paradigms[50, 20, 26] sequentially predict agent trajectories then plan ego motion, but neglect the ego’s impact on others, often yielding over-conservative behaviors. Planning-first paradigms[1, 38] conversely plan ego trajectories before predicting agent responses, risking over-aggressive maneuvers through unrealistic collision-avoidance assumptions. Joint optimization frameworks[53, 35] simultaneously optimize both trajectories with shared objectives, yet suffer from prediction-execution mismatches when agent cooperation assumptions violate real-world responses. Iterative refinement[36, 15], while theoretically optimal for capturing interaction dynamics, incurs prohibitive computational costs for real-time applications. To fully consider the influence of interaction, this paper adapts planning-first paradigm and introduces an interactive regression loss that penalizes trajectory deviations caused by mutual ego-agent influences during optimization.

3 Methodology

EMoE-Planner is a model proposed to address the trajectory planning problem for autonomous driving in urban scenarios. This section provides a detailed introduction to the model, including the specific implementation and the underlying motivations for its design.

3.1 Overview

Problem Description The trajectory planning task in autonomous driving aims to generate safe, comfortable and traffic law-compliant vehicle trajectories for a future time horizon T_f , given the ego vehicle’s state and surrounding environmental information, along with the navigation goal. Let the ego vehicle’s state be denoted as F_e . The surrounding environmental information includes dynamic objects (F_a) such as vehicles and pedestrians, static objects (F_s) such as obstacles and barriers, local map information (F_m), and navigation information (F_{nv}). Given the strong correlation between navigation and map, this work fuses navigation into the map information. The trajectory planning task can be expressed as:

$$\mathcal{T}_{1:T_f} = f(F_e, F_a, F_s, F_m) \quad (1)$$

Where

$$\mathcal{T}_{1:T_f} = \{P_i\}_{i=1:T_f}, P_i = [x_i, y_i, \theta_i, v_i] \quad (2)$$

represents the trajectory points for the next T_f time steps, with each trajectory point P_i consisting of the x and y coordinates, heading angle θ_i , and velocity v_i at the corresponding time step. The EMoE-Planner proposed in this paper serves as the function $f()$ in Equation 1.

Framework Figure 1 illustrates the framework of the proposed model. The model receives the ego vehicle state information $F_e \in R^{D_e}$, dynamic object information $F_a \in R^{N_a \times T_h \times D_a}$, static object information $F_s \in R^{N_s \times D_s}$, and map information $F_m \in R^{N_m \times L_p \times D_m}$. These inputs are processed through respective encoding modules to obtain D-dimensional features, specifically, $[E_{ego} \in R^D, E_{agent} \in R^{N_a \times D}, E_{static} \in R^{N_s \times D}, E_{map} \in R^{N_m \times D}]$. The details of these input encoding modules will be elaborated in Section 3.2. It is worth noting that the positional and heading angle information in the input data are relative values defined in the ego vehicle’s coordinate system.

After encoding, all processed features are concatenated and passed through the scene encoder module, which comprises L_e layers of a normal Transformer encoder, resulting in the scene encoding representation Q_S . Subsequently, Q_S is processed by the EMoE decoder module and the prediction decoder module to generate trajectory queries for the ego vehicle and surrounding vehicles, respectively. These trajectory queries are further processed by the prediction head and the trajectory head to output the predicted trajectories of surrounding vehicles and the planned trajectories for the ego vehicle.

The trajectories for the ego vehicle consist of multiple candidate trajectories, each accompanied by a probability. In the absence of a post-processing module, this work selects the trajectory with the

highest probability as the final planned trajectory, which constitutes the output of the task described by Equation 1. Although predicting trajectories is not the primary objective of this trajectory planning task, it serves as an auxiliary output to supervise the performance of the scene encoder.

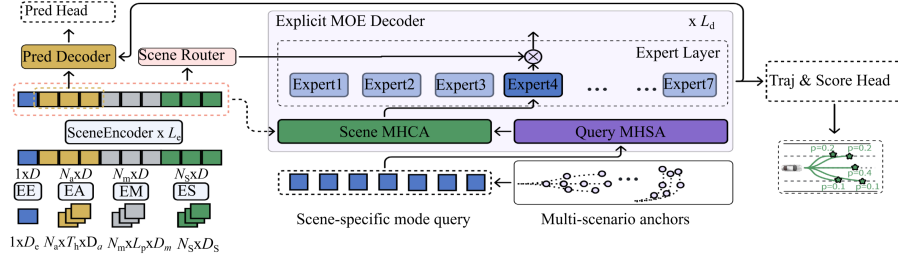


Figure 1: Framework of EMoE-Planner

3.2 Feature Encoders

Ego Status Encoder(EE) & Static Object Encoder(ES) As Equation 3 shows, SDE[7] and multi-layer perceptrons (MLP) are employed to encode F_e and F_s . The ego status $F_e \in R^{D_e}$, where D_e includes positional and heading information, is embedded into dimension D . Similarly, static object information $S \in R^{N_s \times D_s}$, where N_s is the number of static objects and D_s includes attributes such as position, heading, type, and shape, is also embedded into D for concatenation in later stages.

$$E_{ego} = \text{SDE}(F_e), E_{static} = \text{MLP}(F_s) \quad (3)$$

Agent Encoder(EA) & Map Encoder(EM) Unlike EE and ES, the encoding of agent and map information requires consideration of both temporal and spatial compression. Equation 4 shows the process of EA and EM. Raw input of agent is $F_a \in R^{N_a \times T_h \times D_a}$, where N_a is the number of agents, T_h the historical time steps, and D_a encompasses attributes such as position, heading, velocity, shape, and type. Dimension D_a is first embedded into dimension D with Fourier embeddings (FoPE)[21], followed by a compression of N_a to a singular dimension via MLP-Mixer[43]. FoPE effectively capture periodic patterns in the data, facilitating effective temporal compression. Subsequently, the MLP-Mixer employs dual layers of MLPs to perform interactions both within and across the temporal dimension. Similarly, the map information $F_m \in R^{N_m \times L_p \times D_m}$ is also processed with two steps. But the first step is not with foPE but a normal linear layer, which is better to handle spacial information.

$$E_{agent} = \text{MLP-Mixer}(\text{FoPE}(F_a)), E_{map} = \text{MLP-Mixer}(\text{Linear}(F_m)) \quad (4)$$

3.3 Explicit MOE

In our decoder, we incorporate a MoE model, assigning specialized experts to address distinct driving scenarios. In autonomous driving trajectory planning tasks, different scenarios often contain varying types of information, requiring the ego vehicle to focus on specific aspects depending on the situation. Tailoring specific rules for each type of scenarios simplifies them considerably compared to universal rules. By employing specialized experts for varying scenarios in our planning model, we streamline the learning demands for each expert, enhancing the efficiency of the learning process.

Our approach deviates from traditional MoE models by introducing an architecture designed specifically for our task. Figure 2(a) depicts a standard MoE model where at each layer, a router selects top N_E best-suited expert from all experts based on the input information, with $N_E = 1$ in our case, to generate the output. However, this architecture has several limitations: the router lacks explicit constraints, making its selection logic difficult to interpret and prone to confusion in similar scenarios. It also risks an uneven distribution of expert utilization.

Figure 2(b) introduces the explicit MoE (EMoE) architecture developed in this study. Our architecture distinguishes itself by featuring an independent scene router, separate from the expert networks, with a consistent router utilized across all layers. The router inputs are scene features rather than traditional MoE inputs. In trajectory planning tasks, the task scenarios can be explicitly divided into seven categories: turn left at intersections, go straight at intersections, turn right at intersections, go straight at non-intersections, roundabouts, U-turns, and others. Training data is tagged with scene labels, which supervise the output of the scene router. The unified scene router in our EMoE model ensures

that the same expert index is selected for each layer when the scenario type remains consistent. This alignment accelerates model convergence. In contrast, traditional MoE models suffer from reduced training efficiency as they require continuous expert selection due to varying inputs at each layer.

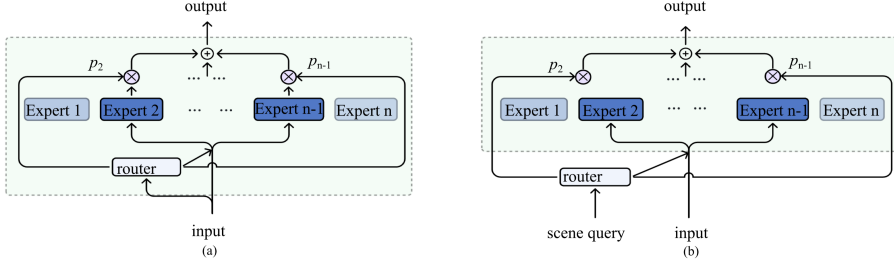


Figure 2: Differences between normal MoE and EMoE

A further benefit of EMoE is the precise control over input data distribution, allowing for a more focused approach to data collection. Notably, less frequent scenarios such as U-turns and roundabouts may yield poorer expert performance due to limited data. To address this, targeted data augmentation for these specific scenarios can be implemented to enhance expert effectiveness.

3.4 Scene-specific query

We introduce scene-specific queries that incorporate prior knowledge at both decision and modality levels, enhancing the model’s focus on future areas relevant to intended actions. This approach not only stabilizes training but also simplifies the learning process. This concept aligns with human driving behaviors where attention is naturally directed towards areas pertinent to intended maneuvers, such as the left-front region when preparing to turn left. As discussed in section 3.3, driving scenarios are categorized into seven types. Utilizing a well-organized dataset, we apply the k-means clustering algorithm to cluster the endpoints of ground-truth trajectories for each scenario type. This results in a set of scene-specific target points denoted as $G \in R^{T \times K_a \times 2}$, with K_a representing the number of clusters and the second dimension representing x and y coordinates. These points, G , serve as anchors analogous to endpoint anchors in existing methodologies. Following scenario classification by the scene router, a specific set of target points $G_i \in R^{K_a \times 2}$ is selected for each scene, facilitating more precise model training and prediction accuracy.

The scene-specific query can be modeled with Equation 5.

$$Q_{\text{mode}} = Q_{\text{learnable}} + \text{FoPE}(G_i) \tag{5}$$

Where $Q_{\text{learnable}} \in R^{K_a \times D}$ is a learnable query. Each Q_{mode} integrates prior knowledge across scenario and modality levels, targeting specific trajectory predictions within designated regions for each scenario. This architecture promotes trajectory generation with multiple modalities while ensuring concentrated attention, thereby stabilizing training and enhancing convergence speed. Moreover, the efficiency of our focused attention mechanism allows for a reduced number of queries (24 in our experiments), in contrast to traditional anchor-based models, leading to more effective region coverage and improved prediction capabilities. Figure 3 shows the distribution of anchor points across the seven scenarios used in our study.

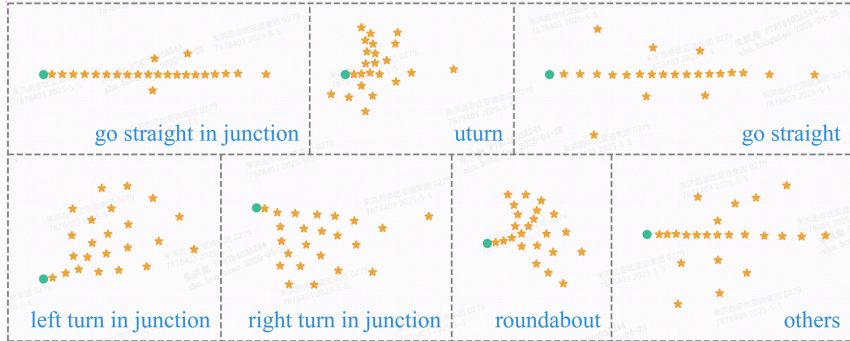


Figure 3: Scene-specific anchors

3.5 Interaction-oriented loss and prediction

3.5.1 Interaction-oriented loss

Temporal-weighted regression loss In existing imitation learning frameworks [6, 7, 47], trajectory regression loss is typically calculated assuming equal importance across all trajectory points, with uniform weighting. However, real-world driving behaviors demonstrate a prioritization of immediate, short-term actions. Nearby obstacles, for instance, may necessitate evasive maneuvers and significantly influence the trajectory, whereas distant obstacles might not alter driving behavior significantly unless they come into closer proximity. This suggests the need for a differentiated approach to learning expert trajectories, where immediate responses to the near-future environment are prioritized over responses to distant conditions.

To better align with these observations, we introduce a temporal-weighted regression loss that scales the importance of each point in a trajectory based on its temporal closeness. The weight for the i -th point is determined by the following formula.

$$w_i = e^{-k_R \times t_i} \quad (6)$$

Where k_R is a hyperparameter used to adjust the weight differences at different time steps, and t_i the temporal distance into the future for the i -th trajectory point.

A notable challenge in imitation learning is the issue of information leakage. This occurs when long-term behaviors in expert trajectories are responses to future events not yet present in the current observable scene. An overemphasis on learning these long-term behaviors can lead to trajectories that are counterintuitive. While the weighting mechanism described in Equation 6 does not completely eliminate the effects of information leakage, it substantially reduces its impact.

Interaction-aware regression Loss In urban environments, the primary complexity arises from interactions between the ego vehicle and other agents, a topic not extensively explored in prior research. Our analysis of closed-loop simulation data from NuPlan reveals that the majority of failures are due to poor interactions between the ego vehicle and other vehicles. In response, this paper introduces an interaction-aware regression loss, which leverages critical interaction periods extracted from the ground truth data to enhance learning in interactive scenarios.

The method for extracting interaction intervals is as follows: traverse each time step t and assess all trajectory points of other agents for potential collisions based on their shapes and orientation angles. Subsequently, using the results from the collision checks, we determine the beginning and ending of interaction intervals, $t_{in}, t_{out} \in [1 : T_f]$. It is essential to clarify that the collisions mentioned herein do not pertain to actual physical interactions between vehicles but rather to instances where two vehicles occupy the same spatial location at different time steps. Furthermore, interaction labels (overtake/yield) are assigned based on the temporal sequence in which the vehicles arrive at the location. Specifically, if the ego vehicle at time t_e "collides" with the i -th vehicle at time t_a , and $t_e < t_a$ (i.e., the ego vehicle passes through first), then $t_{in} = t_e$, and the interacting vehicle is labeled as "overtake".

For the i -th agent, the process of t_{in}^i and t_{out}^i is shown in Equation 7-8. The interaction interval is defined as the union of all (t_{in}^i, t_{out}^i) intervals, as shown in Equation 9.

$$t_{in}^i = \min \left\{ t_{a,i} \mid \exists t_e \in \{1, 2, \dots, T_f\}, \|y_{a,i}^{t_{a,i}} - y_e^{t_e}\| < d_{thr} \right\} \quad (7)$$

$$t_{out}^i = \max \left\{ t_{a,i} \mid \exists t_e \in \{1, 2, \dots, T_f\}, \|y_{a,i}^{t_{a,i}} - y_e^{t_e}\| < d_{thr} \right\} \quad (8)$$

$$(t_{in}, t_{out}) = \bigcup_i (t_{in}^i, t_{out}^i) \quad (9)$$

where $t_{a,i}$ and $y_{a,i}^{t_{a,i}}$ denote the time step and position of the i -th agent, t_e and $y_e^{t_e}$ denote the time step and position of the ego vehicle, d_{thr} is a dynamic threshold at different time steps, depending on the agent size.

Based on the temporal-weighted regression loss in Equation refeq:reg, we set the weights of the ego trajectory points within the interaction intervals to 1 to highlight their importance.

$$w = \begin{cases} 1 & t_{in} \leq t \leq t_{out} \\ e^{-k_R t} & \text{else} \end{cases} \quad (10)$$

The final regression loss can be calculated with Equation 11.

$$\mathcal{L}_{reg} = L1(T_{1:T_f}, T_{1:T_f}^{gt}) \times w_{1:T_f} \quad (11)$$

The overall loss of our model is shown in Equation 12.

$$\mathcal{L} = w_1 \mathcal{L}_{reg} + w_2 \mathcal{L}_{cls} + w_3 \mathcal{L}_{col} + w_4 \mathcal{L}_{pred} + w_5 \mathcal{L}_{router} \quad (12)$$

where w_1, w_2, w_3, w_4 and w_5 are weights of each loss. \mathcal{L}_{cls} , \mathcal{L}_{col} and \mathcal{L}_{pred} are imitation class loss, collision loss and prediction loss. These losses are similar to those in existing work[6, 7], thus we will not introduce them in detail. \mathcal{L}_{router} is the loss of scene router mentioned in section 3.3. It can be calculated with the following equation.

$$\mathcal{L}_{router} = \text{CrossEntropy}(\tau, \tau^{gt}) \quad (13)$$

where, τ is the output of scene router and τ^{gt} is the one-hot distribution derived from the ground truth label of the scenario.

3.5.2 Interaction-oriented prediction

The discourse in Section 2 reveals that prevalent models typically overlook the dynamic interplay between the ego vehicle and other vehicles in trajectory prediction. Recognizing the real-world implications of such interactions, this study integrates the interaction of the ego vehicle’s planned trajectory with those of other vehicles into the prediction framework. As illustrated in Figure 1, this is achieved by introducing a Pred Decoder module. This module synthesizes the agent encoding from the Scene Encoder with the ego vehicle trajectory features from the MOE Decoder via a cross-attention mechanism, facilitating interaction.

While these prediction outcomes do not directly feedback into the decoder or planning module, the interaction fosters enhanced prediction accuracy. This improvement indirectly refines the encoding performance of the Scene Encoder and Feature Encoders, thereby augmenting the overall precision of the trajectory planning process.

4 Experiments

4.1 Experimental Setup

Dataset The training and evaluation of the model were conducted using the NuPlan[3] dataset. From this dataset, 3 million samples, spread across various scenarios, constituted the training sample pool. During preprocessing, samples were categorized into seven scenario types as outlined in Section 3.2. However, not all samples were utilized during the training process. Instead, the size of the training dataset was regulated by controlling the number of each scenario, detailed in Section 4.2.

Benchmark and Metrics The model was evaluated using closed-loop non-reactive (NR) simulations with Val14[11], Test14, and Test14-hard[7] benchmarks. Although NuPlan offers reactive simulations, these are not considered robust due to their simplistic rule-based interactions. The industry uses non-reactive obstacle-based interactions and assigns the main responsibility for collisions, as done in NuPlan’s NR simulations. Therefore, we only use NR as the standard for evaluation. Detailed evaluation metrics can be found in[28].

Baselines The EMOE-Planner was benchmarked against state-of-the-art (SOTA) algorithms categorized into three groups[6]: rule-based, learning-based and hybrid. Algorithms like Pluto and DiffusionPlanner, which integrate rule-based post-processing following a learning-based approach, are classified as hybrid with post-processing while as learning-based without post-processing. Below is the list of baseline algorithms used for comparison.

- IDM[44]– A rule-based trajectory-following method commonly used in planning simulations.
- PDM-Closed[11] – The method uses a common MLP, predicting trajectory with the centerline extracted through IDM and the history of the ego vehicle.
- UrbanDrive[37] – A imitation-learning-based method which train a policy network in closed-loop employing policy gradients.
- PlanTF[7] – A method which applying transformer architecture to imitation learning.
- Pluto[6] – An imitaion learning method with more auxiliary losses and data augmentation.
- DiffusionPlanner[54] – The method achieves the SOTA performance by employing the diffusion model and classifier guidance.

Implementation Details We trained all models on eight Nvidia H800 graphics cards, each with 80GB of VRAM, setting the batch size to 32 and training for 35 epochs. The training time for one million data is approximately 16 hours. The parameters used for training are listed in Table 1.

Table 1: Parameters Used in EMOE-Planner

Name	Description	Values	Name	Description	Values
l_r	learning rate	1e-3	T_f	Future Steps	80
L_e	Num. scene encoder layers	4	T_h	History Steps	20
L_d	Num. decoder layers	4	N_E	Num. experts	7
K_a	Num. anchors	24	k_R	Weight decay factor	0.2
D	Dimention of features	128	D_h	Hidden dim of expert	512

4.2 Results

We assess the performance of all baseline algorithms and EMOE-Planner in NR simulations across Val14, Test14, and Test14-hard. Table 2 presents the evaluation outcomes while Table 3 details the metric results for the top two baseline methods and our method.

Table 2: Closed-loop Results. Higher scores indicate better performance.

Type	Planners	Val14	Test14	Test14-hard
Expert	Log-replay	93.53	94.03	85.96
Rule-based & hybrid	IDM	79.31	70.39	56.15
	PDM-Closed	93.08	90.05	65.08
	Pluto w/ post.	92.88	92.23	80.08
	DiffusionPlanner w/ post.	94.26	94.80	78.87
	EMOE-Planner w/ post. (Ours)	94.35	91.45	80.96
Learning-based	UrbanDriver	67.72	63.27	50.40
	PlanTF	85.30	86.48	69.70
	Pluto w/o post.	89.04	89.90	70.03
	DiffusionPlanner w/o post.	89.87	89.19	75.99
	EMOE-Planner w/o post. (Ours)	93.06	90.67	80.12

According to the results in Table 2, our model outperforms all other learning-based methods across all testing scenarios, particularly excelling in the val14 and test14-hard scenarios where it exceeds the state-of-the-art (SOTA) results by a minimum of 3 points. In the val14 scenarios, the performance of the EMOE-Planner closely approaches that of expert scores. Among rule-based methods, when implementing the same post-processing technique used in Pluto and DiffusionPlanner with our EMOE-Planner, it achieves the highest performance in the val14 and test14-hard scenarios, albeit slightly lower than DiffusionPlanner in the test14 scenario. It is noteworthy that the performance of EMOE-Planner with and without post-processing shows slight differences, suggesting that the trajectories produced by the model are of high quality, potentially diminishing the necessity for post-processing, aligning with our objectives.

As indicated in Table 3, our model generally outperforms both Pluto and DiffusionPlanner in all metrics except speed. Notably, it excels in comfort and progress metrics. The low progress score of Pluto aligns with observations from simulations where Pluto’s trajectories tend to be conservative, often slower than expert trajectories. In the appendix, we provide detailed trajectories for various scenarios to give a comprehensive understanding of the situations discussed here. Our loss function

Table 3: Metrics Results.

Planners	Score	Collisions	TTC	Drivable	Comfort	Progress	Speed
Pluto w/o post.	89.04	96.18	93.28	98.53	96.41	89.56	98.13
DiffusionPlanner	89.87	97.03	94.40	98.74	96.89	91.20	98.11
EMOE-Planner(Ours)	93.06	97.98	94.77	99.54	98.16	92.35	97.87

accounts for vehicle interactions, which effectively optimizes the trajectory progress, particularly in overtaking scenarios, thus avoiding excessive conservatism while preventing collisions.

In the EMOE architecture, the distribution of scenario quantities in the training data is crucial for model performance. Table 4’s second row details the scenario counts in the training dataset. During training, we capped each scenario type at 200,000 from a pool of 3,000,000 samples as discussed in section 4.1. The first four scenario types reached this cap, while the last three did not due to insufficient data in the 3M training database, resulting in a total of 1,083,804 samples used for training. We categorized the scenarios in val14 using the method outlined in the appendix and conducted separate simulation assessments for each scenario type, with results presented in Table 4.

Table 4: Results of different scenarios. ST-J, LT-J, RT-J means go straight, turn left and turn right in junctions. ST means go straight in non-junction areas. UT is u-turn and RA is roundabout.

Scenario Type	ST-J	LT-J	RT-J	UT	ST	RA	Others
Number of Scenarios	200000	200000	200000	17050	200000	105756	160998
NR Score	98.36	93.28	93.60	85.20	91.28	89.33	90.10

Two key insights can be derived from Table 4. Firstly, the quantity of scenarios in the training dataset positively correlates with the expert model’s performance and resulting scores. For instance, scenarios like u-turns and roundabouts, which have fewer instances, exhibit lower scores. Secondly, the complexity of the scene rules affects the model’s learning efficacy, simpler rules, such as those for going straight at an intersection, facilitate better performance. This observation aligns with our expectations. Using scenario-based simulations allows us to identify underperforming scenario types, providing a basis for targeted data enhancement or model optimization in future research.

4.3 Ablation Studies

This section presents ablation studies on three components: EMOE, scene-specific query(SSQ), and interaction-oriented loss and prediction(I-Loss), using the val14 dataset. Table 6 displays the scores following the removal of each module.

Table 5: Ablation experiments.

Version	Score	Collisions	TTC	Drivable	Comfort	Progress	Speed	AvgADE	AvgFDE
Base	93.06	97.98	94.77	99.54	98.16	92.35	97.87	0.71	2.12
w/o EMOE	92.33	97.43	94.49	99.54	98.89	92.26	97.84	0.71	2.12
w/o SSQ	92.51	97.99	95.41	99.17	97.06	91.72	97.92	0.71	2.13
w/o I-Loss	91.44	96.78	93.85	99.72	97.88	91.88	97.89	0.73	2.20

Ablation experiments reveal that interaction-oriented loss and prediction significantly enhance performance, underscoring the importance of interaction. EMOE and scene-specific query also play crucial roles in boosting model performance and these two are used in conjunction. The scene-specific query guides the model’s focus to key scene areas, and EMOE processes that area’s information with a scene-adapted expert. Additionally, Table 5 shows that factoring in interactions yields better predictions for surrounding agents.

5 Conclusion

This paper introduces the EMOE-Planner, a novel framework tailored for enhancing trajectory planning in urban autonomous driving by utilizing scene information and interaction dynamics. The framework employs scene-specific queries generated through multiple scene anchors, focusing the model’s attention on relevant areas. Integration of a Mixture of Experts (MoE) with a shared scene router allows for precise matching of scene types with respective experts, improving the model’s responsiveness to varied scenarios and increasing the transparency of expert selection. Additionally, incorporating interactions between the ego vehicle and other agents into the loss function significantly improves trajectory scoring. Benchmark evaluations on several NuPlan datasets demonstrate that the EMOE-Planner surpasses state-of-the-art (SOTA) models by three points in closed-loop evaluations and closely aligns with the performance of post-processed SOTA methods, reducing reliance on rule-based post-processing.

Acknowledgments and Disclosure of Funding

Funding This work was supported by internal research funds from BYD Company Limited (No external funding was received).

Competing interests All authors are employees of BYD Company Limited. The research represents original work without conflicts of interest.

References

- [1] Sangjae Bae, David Isele, Alireza Nakhaei, Peng Xu, Alexandre Miranda Añon, Chiho Choi, Kikuo Fujimura, and Scott Moura. Lane-change in dense traffic with model predictive control and neural networks. *IEEE Transactions on Control Systems Technology*, 31(2):646–659, 2022.
- [2] Jinze Bai, Shuai Bai, Yunfei Chu, Zeyu Cui, Kai Dang, Xiaodong Deng, Yang Fan, Wenbin Ge, Yu Han, Fei Huang, et al. Qwen technical report. *arXiv preprint arXiv:2309.16609*, 2023.
- [3] Holger Caesar, Juraj Kabzan, Kok Seang Tan, Whye Kit Fong, Eric Wolff, Alex Lang, Luke Fletcher, Oscar Beijbom, and Sammy Omari. nuplan: A closed-loop ml-based planning benchmark for autonomous vehicles. *arXiv preprint arXiv:2106.11810*, 2021.
- [4] Yuning Chai, Benjamin Sapp, Mayank Bansal, and Dragomir Anguelov. Multipath: Multiple probabilistic anchor trajectory hypotheses for behavior prediction. *arXiv preprint arXiv:1910.05449*, 2019.
- [5] Shaoyu Chen, Bo Jiang, Hao Gao, Bencheng Liao, Qing Xu, Qian Zhang, Chang Huang, Wenyu Liu, and Xinggong Wang. Vad2: End-to-end vectorized autonomous driving via probabilistic planning. *arXiv preprint arXiv:2402.13243*, 2024.
- [6] Jie Cheng, Yingbing Chen, and Qifeng Chen. Pluto: Pushing the limit of imitation learning-based planning for autonomous driving. *arXiv preprint arXiv:2404.14327*, 2024.
- [7] Jie Cheng, Yingbing Chen, Xiaodong Mei, Bowen Yang, Bo Li, and Ming Liu. Rethinking imitation-based planners for autonomous driving. In *2024 IEEE International Conference on Robotics and Automation (ICRA)*, pages 14123–14130. IEEE, 2024.
- [8] Jie Cheng, Ren Xin, Sheng Wang, and Ming Liu. Mpnnp: Multi-policy neural planner for urban driving. In *2022 IEEE/RSJ International Conference on Intelligent Robots and Systems (IROS)*, pages 10549–10554. IEEE, 2022.
- [9] Kashyap Chitta, Aditya Prakash, Bernhard Jaeger, Zehao Yu, Katrin Renz, and Andreas Geiger. Transfuser: Imitation with transformer-based sensor fusion for autonomous driving. *IEEE transactions on pattern analysis and machine intelligence*, 45(11):12878–12895, 2022.
- [10] Alexander G Cunningham, Enric Galceran, Ryan M Eustice, and Edwin Olson. Mpdm: Multipolicy decision-making in dynamic, uncertain environments for autonomous driving. In *2015 IEEE International Conference on Robotics and Automation (ICRA)*, pages 1670–1677. IEEE, 2015.
- [11] Daniel Dauner, Marcel Hallgarten, Andreas Geiger, and Kashyap Chitta. Parting with misconceptions about learning-based vehicle motion planning. In *Conference on Robot Learning*, pages 1268–1281. PMLR, 2023.
- [12] Dmitri Dolgov, Sebastian Thrun, Michael Montemerlo, and James Diebel. Practical search techniques in path planning for autonomous driving. *ann arbor*, 1001(48105):18–80, 2008.
- [13] Liangji Fang, Qinhong Jiang, Jianping Shi, and Bolei Zhou. Tpnnet: Trajectory proposal network for motion prediction. In *Proceedings of the IEEE/CVF conference on computer vision and pattern recognition*, pages 6797–6806, 2020.
- [14] William Fedus, Barret Zoph, and Noam Shazeer. Switch transformers: Scaling to trillion parameter models with simple and efficient sparsity. *Journal of Machine Learning Research*, 23(120):1–39, 2022.

- [15] Enric Galceran, Alexander G Cunningham, Ryan M Eustice, and Edwin Olson. Multipolicy decision-making for autonomous driving via changepoint-based behavior prediction: Theory and experiment. *Autonomous Robots*, 41:1367–1382, 2017.
- [16] Thomas Gilles, Stefano Sabatini, Dzmitry Tsishkou, Bogdan Stanciulescu, and Fabien Moutarde. Home: Heatmap output for future motion estimation. In *2021 IEEE International Intelligent Transportation Systems Conference (ITSC)*, pages 500–507. IEEE, 2021.
- [17] Thomas Gilles, Stefano Sabatini, Dzmitry Tsishkou, Bogdan Stanciulescu, and Fabien Moutarde. Gohome: Graph-oriented heatmap output for future motion estimation. In *2022 international conference on robotics and automation (ICRA)*, pages 9107–9114. IEEE, 2022.
- [18] Joey Hong, Benjamin Sapp, and James Philbin. Rules of the road: Predicting driving behavior with a convolutional model of semantic interactions. In *Proceedings of the IEEE/CVF Conference on Computer Vision and Pattern Recognition*, pages 8454–8462, 2019.
- [19] Yihan Hu, Siqi Chai, Zhenning Yang, Jingyu Qian, Kun Li, Wenxin Shao, Haichao Zhang, Wei Xu, and Qiang Liu. Solving motion planning tasks with a scalable generative model. In *European Conference on Computer Vision*, pages 386–404. Springer, 2024.
- [20] Yihan Hu, Jiazhi Yang, Li Chen, Keyu Li, Chonghao Sima, Xizhou Zhu, Siqi Chai, Senyao Du, Tianwei Lin, Wenhai Wang, et al. Planning-oriented autonomous driving. In *Proceedings of the IEEE/CVF conference on computer vision and pattern recognition*, pages 17853–17862, 2023.
- [21] Ermo Hua, Che Jiang, Xingtai Lv, Kaiyan Zhang, Ning Ding, Youbang Sun, Biqing Qi, Yuchen Fan, Xuekai Zhu, and Bowen Zhou. Fourier position embedding: Enhancing attention’s periodic extension for length generalization. *arXiv preprint arXiv:2412.17739*, 2024.
- [22] Zhiyu Huang, Peter Karkus, Boris Ivanovic, Yuxiao Chen, Marco Pavone, and Chen Lv. Dtp: Differentiable joint conditional prediction and cost evaluation for tree policy planning in autonomous driving. In *2024 IEEE International Conference on Robotics and Automation (ICRA)*, pages 6806–6812. IEEE, 2024.
- [23] Zhiyu Huang, Haochen Liu, and Chen Lv. Gameformer: Game-theoretic modeling and learning of transformer-based interactive prediction and planning for autonomous driving. In *Proceedings of the IEEE/CVF International Conference on Computer Vision*, pages 3903–3913, 2023.
- [24] Zhiyu Huang, Xinshuo Weng, Maximilian Igl, Yuxiao Chen, Yulong Cao, Boris Ivanovic, Marco Pavone, and Chen Lv. Gen-drive: Enhancing diffusion generative driving policies with reward modeling and reinforcement learning fine-tuning. *arXiv preprint arXiv:2410.05582*, 2024.
- [25] Robert A Jacobs, Michael I Jordan, Steven J Nowlan, and Geoffrey E Hinton. Adaptive mixtures of local experts. *Neural computation*, 3(1):79–87, 1991.
- [26] Bo Jiang, Shaoyu Chen, Qing Xu, Bencheng Liao, Jiajie Chen, Helong Zhou, Qian Zhang, Wenyu Liu, Chang Huang, and Xinggang Wang. Vad: Vectorized scene representation for efficient autonomous driving. In *Proceedings of the IEEE/CVF International Conference on Computer Vision*, pages 8340–8350, 2023.
- [27] Chiyu Jiang, Andre Cornman, Cheolho Park, Benjamin Sapp, Yin Zhou, Dragomir Anguelov, et al. Motiodiffuser: Controllable multi-agent motion prediction using diffusion. In *Proceedings of the IEEE/CVF conference on computer vision and pattern recognition*, pages 9644–9653, 2023.
- [28] Napat Karnchanachari, Dimitris Geromichalos, Kok Seang Tan, Nanxiang Li, Christopher Eriksen, Shakiba Yaghoubi, Noushin Mehdipour, Gianmarco Bernasconi, Whye Kit Fong, Yiluan Guo, et al. Towards learning-based planning: The nuPlan benchmark for real-world autonomous driving. In *2024 IEEE International Conference on Robotics and Automation (ICRA)*, pages 629–636. IEEE, 2024.
- [29] Dmitry Lepikhin, HyoukJoong Lee, Yuanzhong Xu, Dehao Chen, Orhan Firat, Yanping Huang, Maxim Krikun, Noam Shazeer, and Zhifeng Chen. Gshard: Scaling giant models with conditional computation and automatic sharding. *arXiv preprint arXiv:2006.16668*, 2020.

- [30] Zhenxin Li, Kailin Li, Shihao Wang, Shiyi Lan, Zhiding Yu, Yishen Ji, Zhiqi Li, Ziyue Zhu, Jan Kautz, Zuxuan Wu, et al. Hydra-mdp: End-to-end multimodal planning with multi-target hydra-distillation. *arXiv preprint arXiv:2406.06978*, 2024.
- [31] Ming Liang, Bin Yang, Rui Hu, Yun Chen, Renjie Liao, Song Feng, and Raquel Urtasun. Learning lane graph representations for motion forecasting. In *Computer Vision–ECCV 2020: 16th European Conference, Glasgow, UK, August 23–28, 2020, Proceedings, Part II 16*, pages 541–556. Springer, 2020.
- [32] Bencheng Liao, Shaoyu Chen, Haoran Yin, Bo Jiang, Cheng Wang, Sixu Yan, Xinbang Zhang, Xiangyu Li, Ying Zhang, Qian Zhang, et al. Diffusiondrive: Truncated diffusion model for end-to-end autonomous driving. *arXiv preprint arXiv:2411.15139*, 2024.
- [33] Aixin Liu, Bei Feng, Bin Wang, Bingxuan Wang, Bo Liu, Chenggang Zhao, Chengqi Deng, Chong Ruan, Damai Dai, Daya Guo, et al. Deepseek-v2: A strong, economical, and efficient mixture-of-experts language model. *arXiv preprint arXiv:2405.04434*, 2024.
- [34] Yicheng Liu, Jinghui Zhang, Liangji Fang, Qinhong Jiang, and Bolei Zhou. Multimodal motion prediction with stacked transformers. In *Proceedings of the IEEE/CVF conference on computer vision and pattern recognition*, pages 7577–7586, 2021.
- [35] Stefano Pini, Christian S Perone, Aayush Ahuja, Ana Sofia Rufino Ferreira, Moritz Niendorf, and Sergey Zagoruyko. Safe real-world autonomous driving by learning to predict and plan with a mixture of experts. In *2023 IEEE International Conference on Robotics and Automation (ICRA)*, pages 10069–10075. IEEE, 2023.
- [36] Nicholas Rhinehart, Jeff He, Charles Packer, Matthew A Wright, Rowan McAllister, Joseph E Gonzalez, and Sergey Levine. Contingencies from observations: Tractable contingency planning with learned behavior models. In *2021 IEEE International Conference on Robotics and Automation (ICRA)*, pages 13663–13669. IEEE, 2021.
- [37] Oliver Scheel, Luca Bergamini, Maciej Wolczyk, Błażej Osipiński, and Peter Ondruska. Urban driver: Learning to drive from real-world demonstrations using policy gradients. In *Conference on Robot Learning*, pages 718–728. PMLR, 2022.
- [38] Zihao Sheng, Lin Liu, Shibe Xue, Dezong Zhao, Min Jiang, and Dewei Li. A cooperation-aware lane change method for automated vehicles. *IEEE Transactions on Intelligent Transportation Systems*, 24(3):3236–3251, 2022.
- [39] Shaoshuai Shi, Li Jiang, Dengxin Dai, and Bernt Schiele. Motion transformer with global intention localization and local movement refinement. *Advances in Neural Information Processing Systems*, 35:6531–6543, 2022.
- [40] Chonghao Sima, Katrin Renz, Kashyap Chitta, Li Chen, Hanxue Zhang, Chengen Xie, Jens Beißwenger, Ping Luo, Andreas Geiger, and Hongyang Li. Drivelm: Driving with graph visual question answering. In *European Conference on Computer Vision*, pages 256–274. Springer, 2024.
- [41] Qiao Sun, Huimin Wang, Jiahao Zhan, Fan Nie, Xin Wen, Leimeng Xu, Kun Zhan, Peng Jia, Xianpeng Lang, and Hang Zhao. Generalizing motion planners with mixture of experts for autonomous driving. *arXiv preprint arXiv:2410.15774*, 2024.
- [42] Qiao Sun, Shiduo Zhang, Danjiao Ma, Jingzhe Shi, Derun Li, Simian Luo, Yu Wang, Ningyi Xu, Guangzhi Cao, and Hang Zhao. Large trajectory models are scalable motion predictors and planners. *arXiv preprint arXiv:2310.19620*, 2023.
- [43] Ilya O Tolstikhin, Neil Houlsby, Alexander Kolesnikov, Lucas Beyer, Xiaohua Zhai, Thomas Unterthiner, Jessica Yung, Andreas Steiner, Daniel Keysers, Jakob Uszkoreit, et al. Mlp-mixer: An all-mlp architecture for vision. *Advances in neural information processing systems*, 34:24261–24272, 2021.
- [44] Martin Treiber, Ansgar Hennecke, and Dirk Helbing. Congested traffic states in empirical observations and microscopic simulations. *Physical review E*, 62(2):1805, 2000.

- [45] Ashish Vaswani, Noam Shazeer, Niki Parmar, Jakob Uszkoreit, Llion Jones, Aidan N. Gomez, Lukasz Kaiser, and Illia Polosukhin. Attention is all you need, 2023.
- [46] Tianwen Wei, Bo Zhu, Liang Zhao, Cheng Cheng, Biye Li, Weiwei Lü, Peng Cheng, Jianhao Zhang, Xiaoyu Zhang, Liang Zeng, et al. Skywork-moe: A deep dive into training techniques for mixture-of-experts language models. *arXiv preprint arXiv:2406.06563*, 2024.
- [47] Ren Xin, Jie Cheng, Hongji Liu, and Jun Ma. Planscope: Learning to plan within decision scope does matter. *arXiv preprint arXiv:2411.00476*, 2024.
- [48] Zebin Xing, Xingyu Zhang, Yang Hu, Bo Jiang, Tong He, Qian Zhang, Xiaoxiao Long, and Wei Yin. Goalflow: Goal-driven flow matching for multimodal trajectories generation in end-to-end autonomous driving. *arXiv preprint arXiv:2503.05689*, 2025.
- [49] Takuma Yagi, Karttikeya Mangalam, Ryo Yonetani, and Yoichi Sato. Future person localization in first-person videos. In *Proceedings of the IEEE Conference on Computer Vision and Pattern Recognition*, pages 7593–7602, 2018.
- [50] Wenyuan Zeng, Wenjie Luo, Simon Suo, Abbas Sadat, Bin Yang, Sergio Casas, and Raquel Urtasun. End-to-end interpretable neural motion planner. In *Proceedings of the IEEE/CVF conference on computer vision and pattern recognition*, pages 8660–8669, 2019.
- [51] Lu Zhang, Wenchao Ding, Jing Chen, and Shaojie Shen. Efficient uncertainty-aware decision-making for automated driving using guided branching. In *2020 IEEE International Conference on Robotics and Automation (ICRA)*, pages 3291–3297. IEEE, 2020.
- [52] Hang Zhao, Jiyang Gao, Tian Lan, Chen Sun, Ben Sapp, Balakrishnan Varadarajan, Yue Shen, Yi Shen, Yuning Chai, Cordelia Schmid, et al. Tnt: Target-driven trajectory prediction. In *Conference on Robot Learning*, pages 895–904. PMLR, 2021.
- [53] Wenzhao Zheng, Ruiqi Song, Xianda Guo, Chenming Zhang, and Long Chen. Genad: Generative end-to-end autonomous driving. In *European Conference on Computer Vision*, pages 87–104. Springer, 2024.
- [54] Yinan Zheng, Ruiming Liang, Kexin Zheng, Jinliang Zheng, Liyuan Mao, Jianxiong Li, Weihao Gu, Rui Ai, Shengbo Eben Li, Xianyuan Zhan, et al. Diffusion-based planning for autonomous driving with flexible guidance. *arXiv preprint arXiv:2501.15564*, 2025.

A Supplementary Material

Figures 4 through 7 illustrate the closed-loop simulation results for four distinct scenarios. We present snapshots at 0s, 5s, 10s, and 15s for both Pluto and EMOE-Planner. In Figure 4(b), it is clear that Pluto collides with a stationary vehicle during a right turn, while EMOE-Planner navigates a safe trajectory. The trajectory by EMOE-Planner in Figure 4(f) initially aligns more closely with the ground truth, attributable to the incorporation of temporal-weighted regression loss, which prioritizes near-term planning and enhances learning from the expert’s obstacle avoidance maneuvers. Conversely, Pluto prioritizes overall trajectory resemblance to the expert, potentially compromising local accuracy for global alignment, leading to less optimal near-term planning.

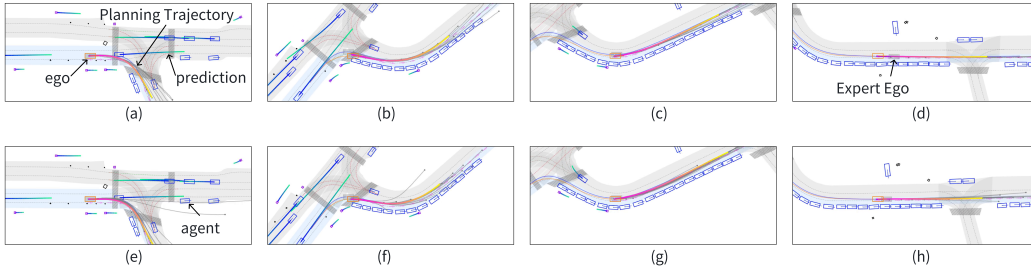


Figure 4: Closed-loop simulation in scenario1. Subfigures (a) through (d) depict snapshots at 0s, 5s, 10s, and 15s for Pluto, while subfigures (e) through (h) represent snapshots at corresponding times for EMOE-Planner.

In the scenario depicted in Figure 5, Pluto halts at the intersection instead of executing the expected right turn, while EMOE-Planner successfully completes it. The reason for Pluto’s halt is difficult to ascertain; however, it is evident that the expert network in EMOE-Planner more effectively manages such irregular scenarios.

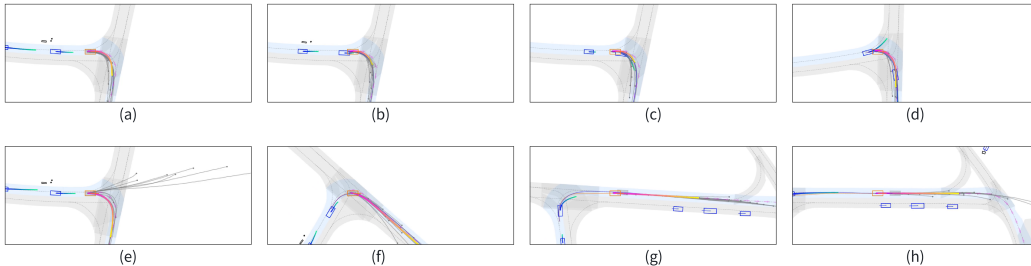


Figure 5: Closed-loop simulation in scenario2.

Figure 6 depicts a right turn at a busy intersection, where both Pluto and EMOE-Planner execute the maneuver correctly. However, Figure 6(b) shows that Pluto adopts a notably cautious approach, trailing almost one car length behind the expert at 5 seconds, and by Figures 6(d), it falls approximately 15 meters behind by 15 seconds. In contrast, EMOE-Planner is only about 7 meters behind in Figure 6(h). Pluto’s trajectory does not account for interactions with other vehicles, leading to a safer but more conservative path, while EMOE-Planner’s interaction-aware planning yields a trajectory closer to that of the expert.

In Figure 7, the scenario involves driving straight through an intersection. Here, Pluto unnecessarily changes lanes mid-intersection likely due to a perceived collision threat from the vehicle in the red box in Figure (b), prompting a lane change that is reversed in Figure 7(c). EMOE-Planner, however, evaluates the collision potential more accurately, maintaining a straight trajectory and successfully navigating the intersection. However, although EMOE-Planner proceeds straight, the trajectory remains conservative due to the high traffic in the scenario. The current framework does not yet consider the prediction of other vehicles when planning the ego vehicle’s trajectory, which will be a focus of our future work.

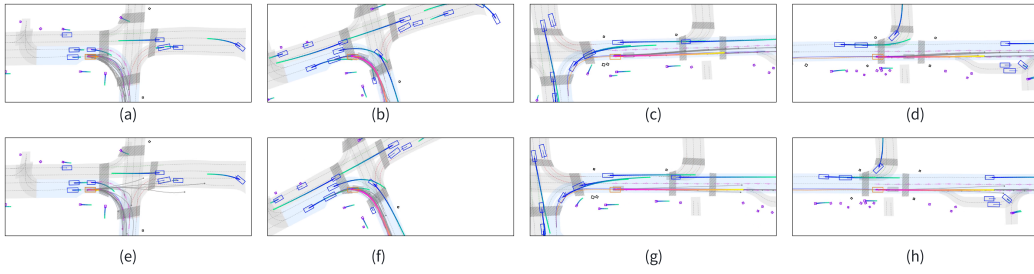


Figure 6: Closed-loop simulation in scenario3.

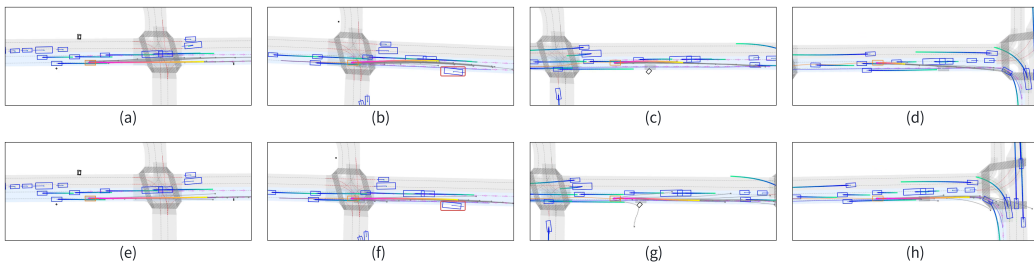


Figure 7: Closed-loop simulation in scenario4.